The American Journal of Human Genetics, *91*

Supplemental Data

Alteration of Fatty-Acid-Metabolizing Enzymes Affects Mitochondrial Form and Function in Hereditary Spastic Paraplegia

Christelle Tesson, Magdalena Nawara, Mustafa A. M. Salih, Rodrigue Rossignol, Maha S. Zaki, Mohammed Al Balwi, Rebecca Schule, Cyril Mignot, Emilie Obre, Ahmed Bouhouche, Filippo M. Santorelli, Christelle M. Durand, Andrés Caballero Oteyza, Khalid H. El-Hachimi, Abdulmajeed AlDrees, Naima Bouslam, Foudil Lamari, Salah A. Elmalik, Mohammad M. Kabiraj, Mohammed Z. Seidahmed, Typhaine Esteves, Marion Gaussen, Marie-Lorraine Monin, Gabor Gyapay, Doris Lechner, Michael Gonzalez, Christel Depienne, Fanny Mochel, Julie Lavie, Ludger Schols, Didier Lacombe, Mohamed Yahyaoui, Ibrahim Al Abdulkareem, Stephan Zuchner, Atsushi Yamashita, Ali Benomar, Cyril Goizet, Alexandra Durr, Joseph G. Gleeson, Frederic Darios, Alexis Brice, and Giovanni Stevanin

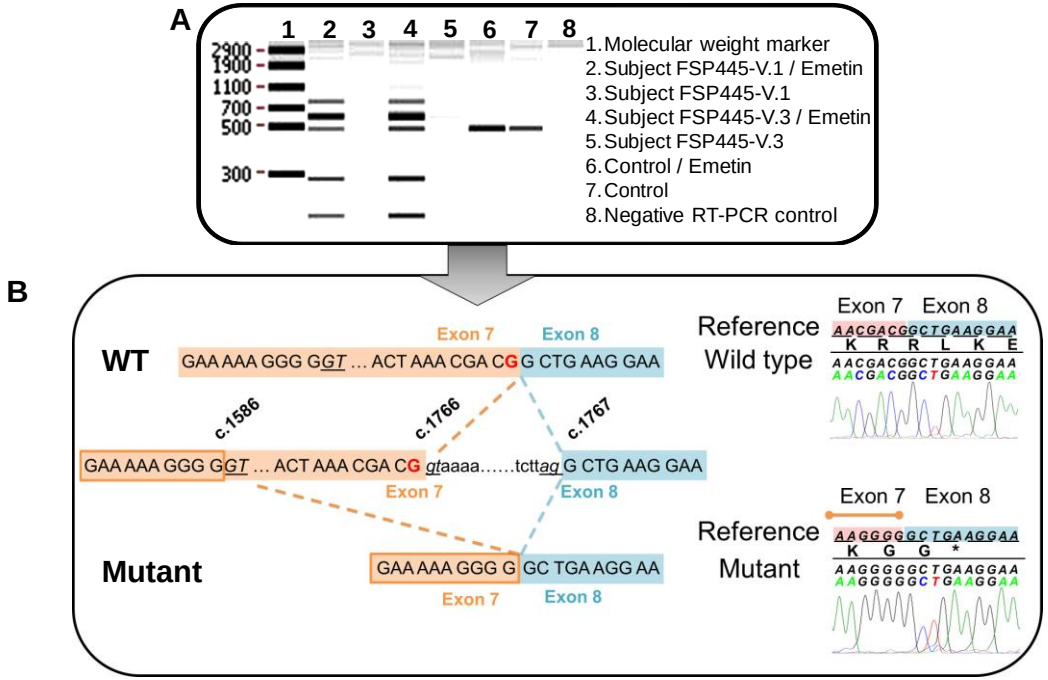

Figure S1. Abnormal Splicing of *DDHD1* Evidenced in Lymphoblasts of SPG28-Affected Subjects from Family FSP445

To verify the consequences of the c.1766G>A variant in *DDHD1* in affected members of the family, we extracted mRNA from lymphoblastoid cell lines of subjects FSP445-V.1 and –V.3 in presence or absence of emetin which blocks non-sense mediated mRNA decay.

(A) The result of cDNA amplification of the affected individuals and one control with primers flanking the splice site junction in exons 6 and 8, shows the presence of the wild type transcript in the control individual and multiple bands of higher and lower molecular weight in both affected subjects, but only after treatment of cells with emetin. The image was acquired with the LabChip GX (Caliper). This finding suggests that the mutation leads to abnormal splicing by revealing multiple cryptic donor sites.

(B) A fraction of the abnormal PCR products were subcloned and sequenced and confirmed the aberrant splicing of *DDHD1* in affected individuals. The graphic representation of *DDHD1* compares the splicing in a wild type control and in one of the cloned PCR products from cDNA of a mutated subject (gel line A-4). The incorrect splicing results in the generation of a premature STOP codon introduction (TGA). The splice donor and acceptor sites are shown in italics and underlined. The wild-type version of the mutated base is depicted in red.

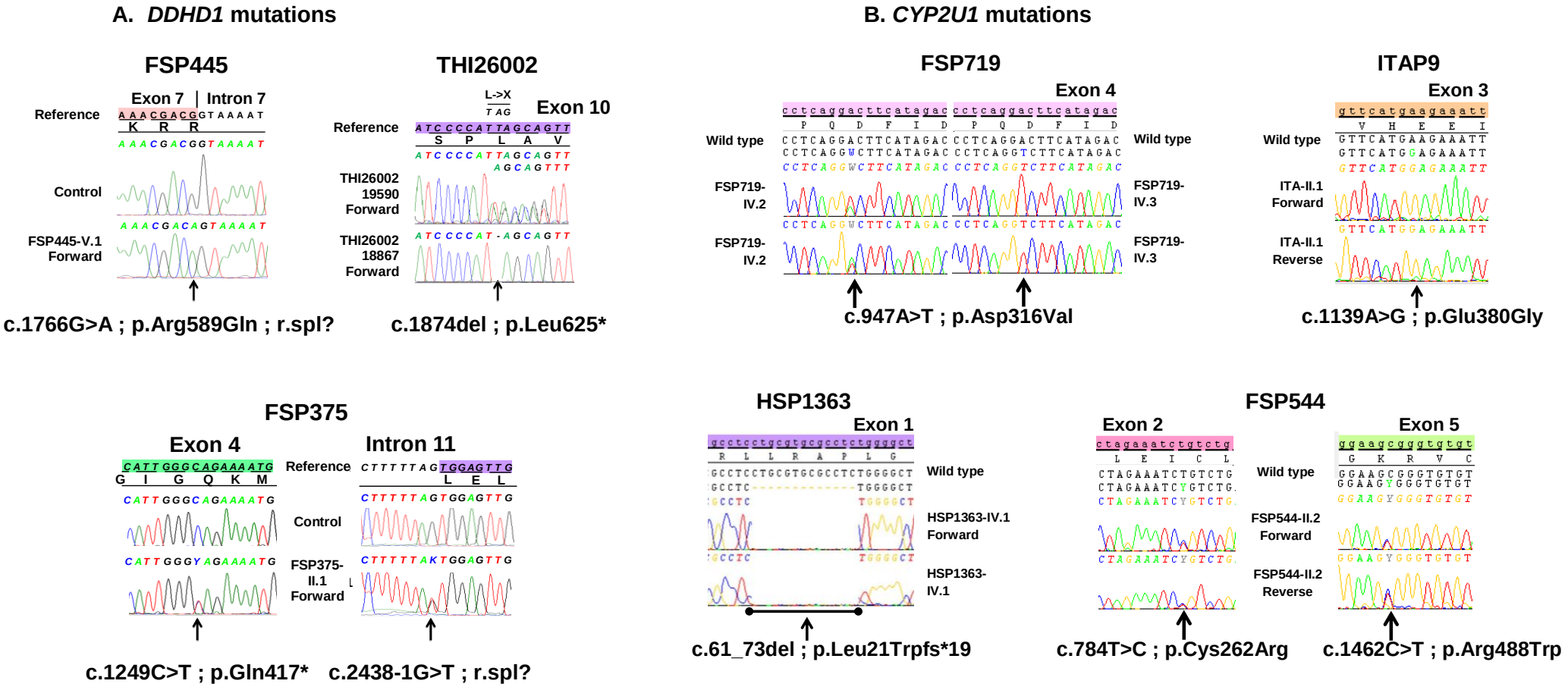

Figure S2. Electrophoregrams in Individuals with *DDHD1* or *CYP2U1* Mutations

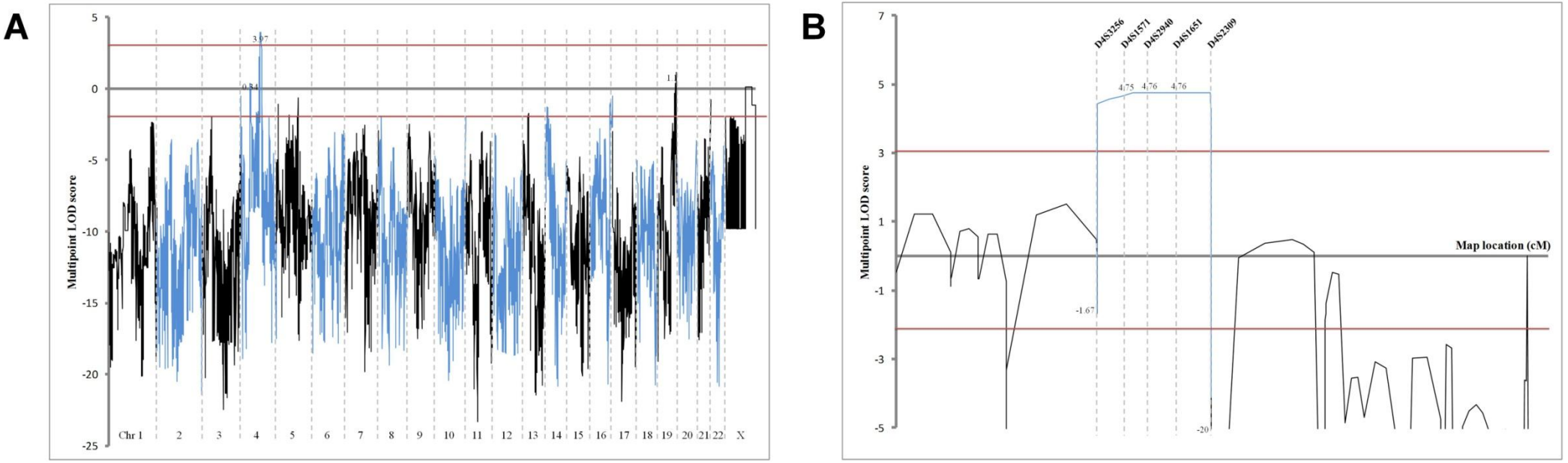

Figure S3. Multipoint LOD Score Plots in Family FSP719

(A) Multipoint LOD score plot of the genome-wide linkage analysis performed in Family FSP719. A genome scan using the Illumina LINKAGE Mapping V SNP set was performed in all sampled individuals (*). Multipoint LOD scores were calculated using Merlin 1.0 and identified three genomic regions on chromosomes 4, 19 and X with uninformative multipoint LOD score values between 0 and +1.1 that were excluded using 23 additional markers. A fourth region of 34 consecutive SNPs located on chromosome 4 presented a multipoint LOD score of +3.97 between markers *rs1528381* and *rs1525760*.

(B) Multipoint LOD score plot after genotyping of 24 additional microsatellite markers in family FSP719, which confirmed a 5.9 Mb (6.29 cM) region of linkage of the disease locus between markers *D4S3256* and *D4S2309* with a maximal multipoint LOD score of +4.76.

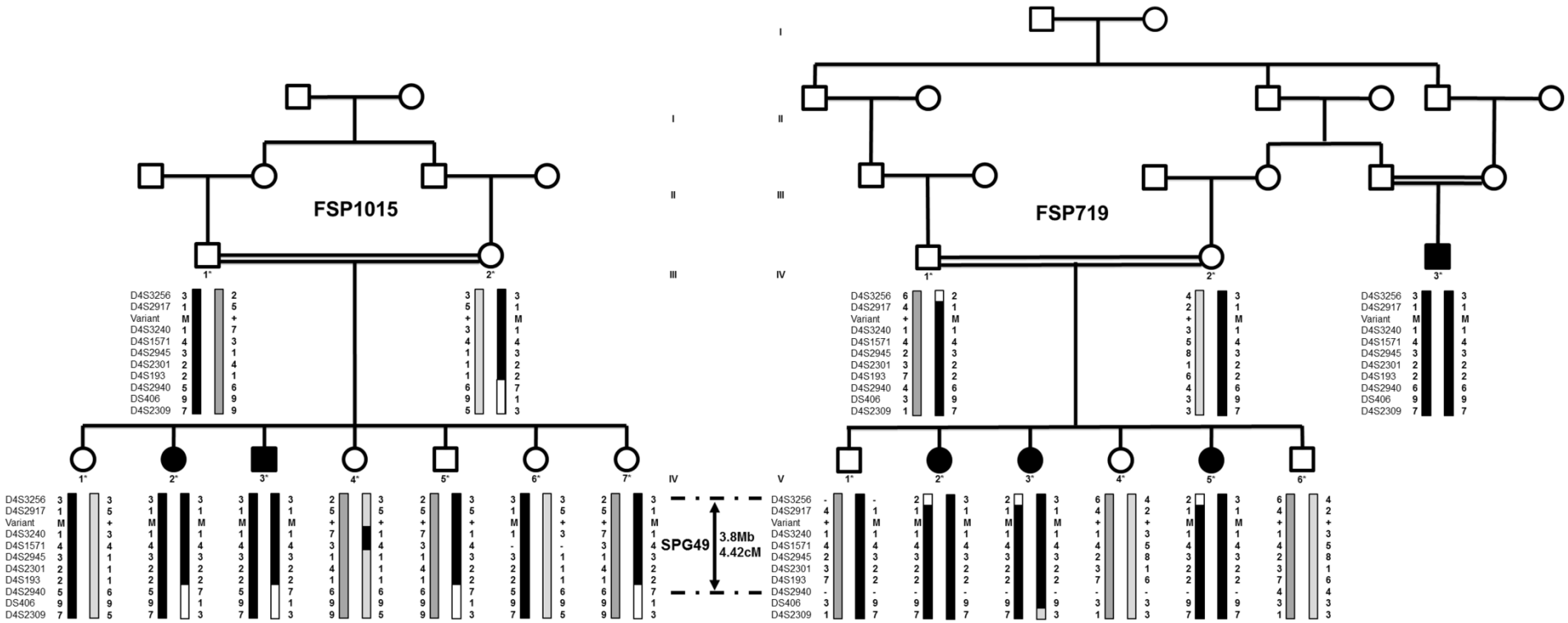

Figure S4. Haplotypes Segregating in Chromosome 4 in Two SPG49 Families

Refinement of the *SPG49* interval by genotyping of 10 microsatellite markers in two AR-HSP families with the same geographic origin (Saudi Arabia) and from the same tribe. Both SPG49 families shared a portion of the same homozygous haplotype, suggesting a common ancestry. We considered the 3.8 Mb (4.42 cM) interval between markers *D4S3256* and *D4S2940* as the restricted SPG49 disease locus. Regions of homozygosity are indicated by black bars. The variant c.947A>T in *CYP2U1* is also indicated in the haplotypes. *, sampled individuals.

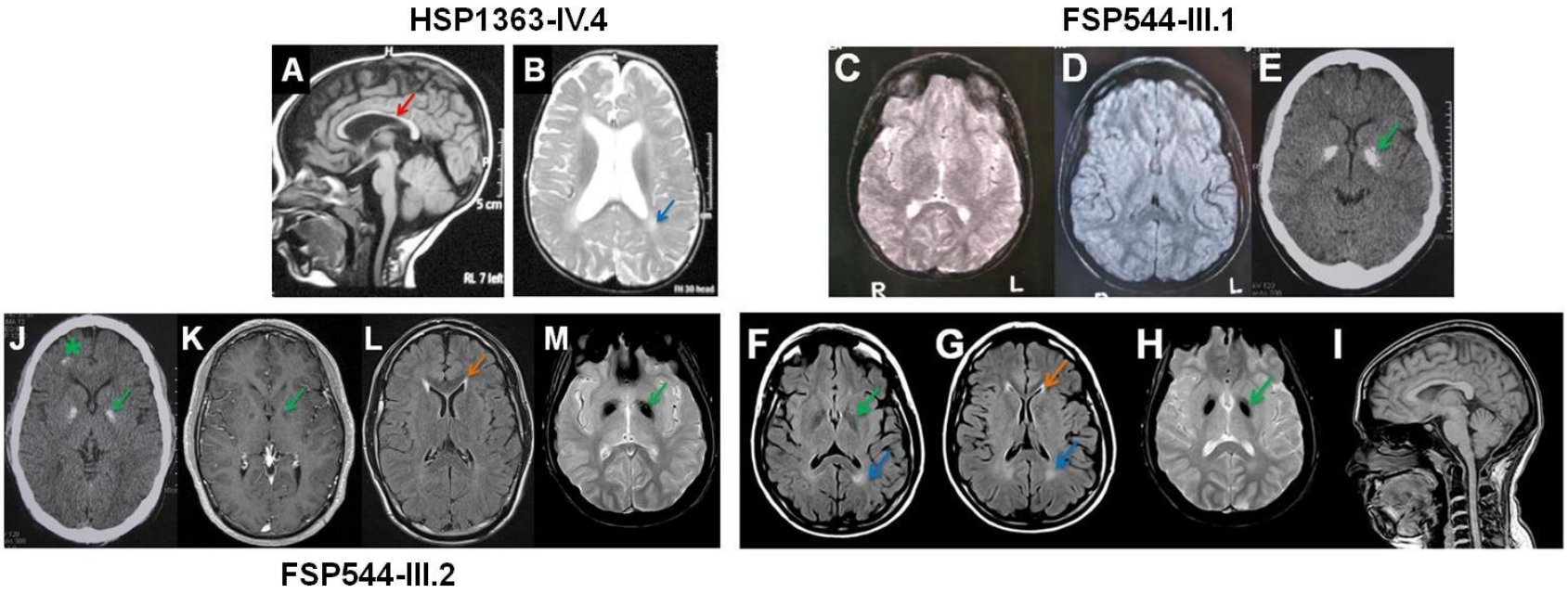

Figure S5. **Neuroradiological Examinations of Three SPG49 Individuals**

(A and B) Cerebral MRI images from individual HSP1363-IV.4 at age 2.5 years, after 2.5 years of disease evolution. (A) T1-weighted sagittal view shows atrophy of the corpus callosum (red arrow) and (B) T2-weighted axial view shows hyperintense periventricular white matter (blue arrow).

(C–I) radiological examinations of individual FSP544-III.1. T2 (C) and FLAIR (D) brain MRI axial scans show no obvious abnormality at 14 years of age. At 30 years old, a CT scan (E) shows bilateral globus pallidus calcifications (green arrow) and a brain MRI (F to I) shows 1) heterogeneous T1 hypointensity of both globus pallidus (F, green arrow); 2) white matter abnormalities (ground glass aspect) (F and G, blue arrows) including the “ear of the lynx” aspect of frontal horns of the lateral ventricles (G, orange arrow), 3) strong hypointensity in T2* axial scan (H, green arrow) but 4) no atrophy of the corpus callosum, cerebral or cerebellar cortex, and pons (I).

(J –M) radiological examinations of subject FSP544-III.2 (25 years old). (J) axial CT scan shows globus pallidus calcifications (green arrow) and focal calcification in the right frontal lobe (*). T1 (K) and T2* (M) brain MRI axial scans show hypointensity of both globus pallidus (green arrows). A ground glass aspect of the white matter is observed in the FLAIR axial scan (L) with the “ears of lynx“ aspect of the frontal horns of lateral ventricules (L, orange arrow).

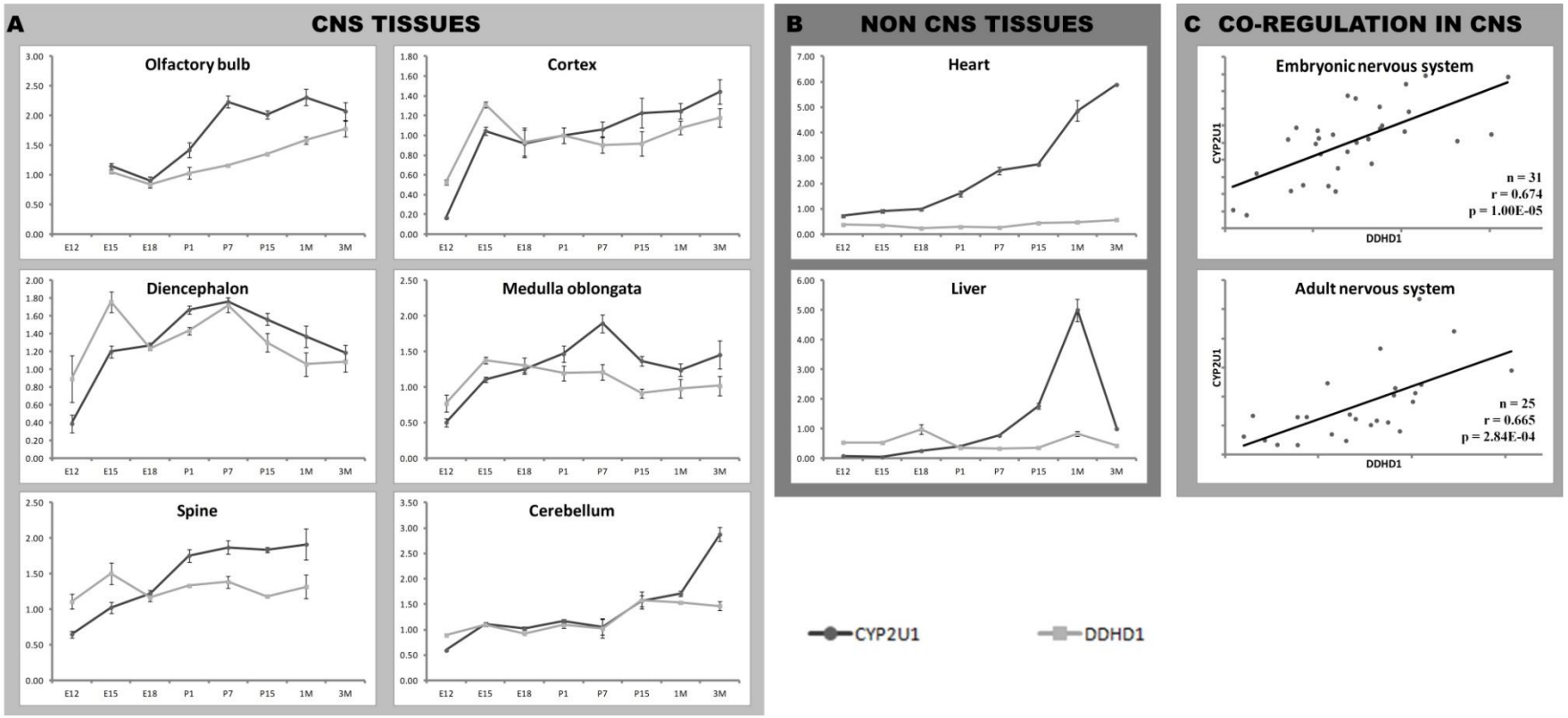

FigureS6. Comparative Expression of *CYP2U1* and *DDHD1* in Developing and Adult Mouse Tissues and their Coregulation in CNS Tissues

(A and B) Expression levels in mouse tissues were evaluated in triplicate samples of four different mice at several developmental stages (E12, E15, E18, P1, P7, P15, 1 month and 3 months) by real-time PCR. Quantification of each sample was carried out using the Qiagen QuantiTect primer assays for *CYP2U1* and *DDHD1*. *PPIA* and *PGK1* were used as control genes. Forty-five two-step cycles (15 seconds at 95°C and 30 seconds at 60°C) were used on a Lightcycler-1536 apparatus (Roche). Analysis was performed using qbase Plus software (Biogazelle). Expression of both genes increased during development, except in peripheral tissues (heart and liver) in the case of *DDHD1*.

(**C**) Expression of both genes are co-regulated in CNS tissues as shown by their correlations (p value in the figures). Each point corresponds to the mean value of the triplicate measures of the expression level performed for both genes. The expression of *DDHD1* and *CYP2U1* in CNS tissues was not significantly co-regulated with the non-related gene *RAD51* (p>0.5, data not shown).

Error bars represent the SD.

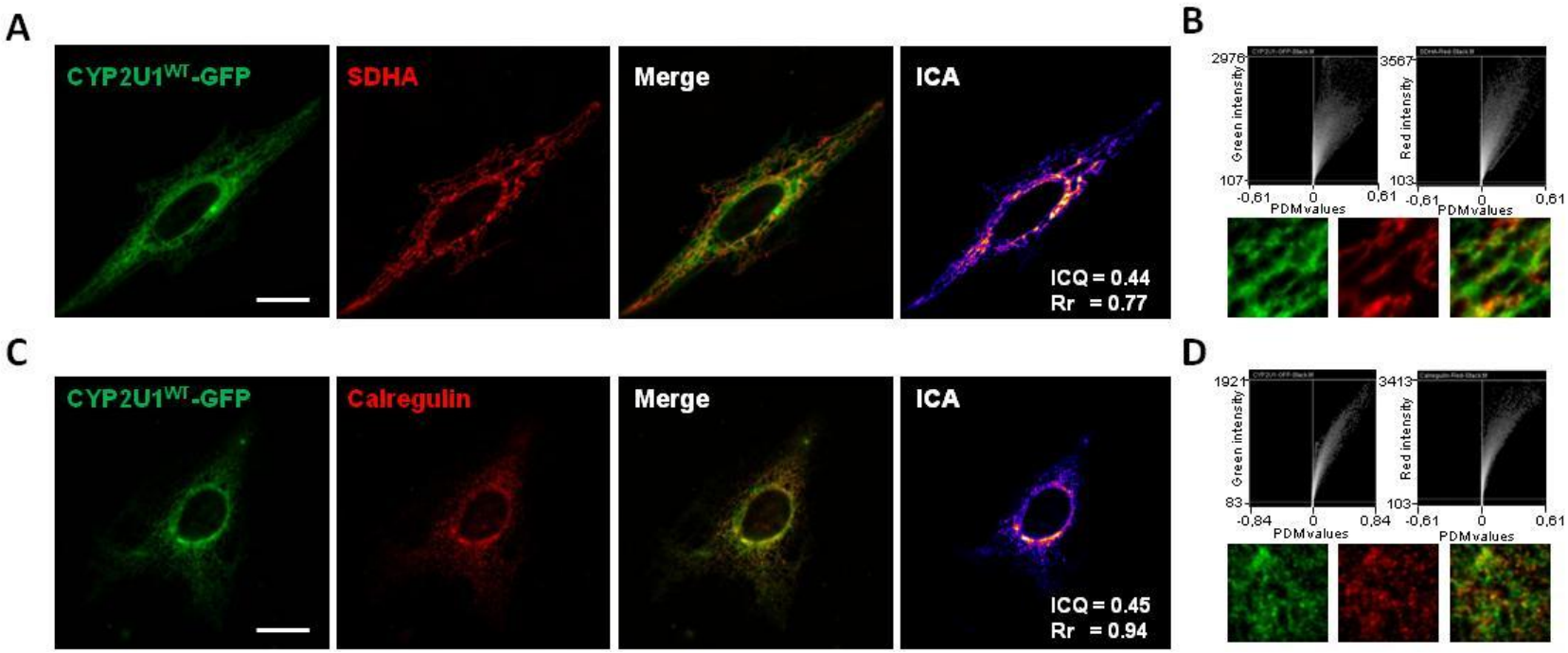

Figure S7. Subcellular Distribution Profile of CYP2U1

(A and C) Overexpression of a CYP2U1-GFP fusion protein (green) was performed in HeLa cells and costaining was performed with an antibody against the mitochondrial inner-membrane marker SDHA (A, red) or the endoplasmic reticulum (ER) marker Calregulin (C, red). 3D-Images were obtained using a Zeiss Vivatome microscope (objectives x63, scale bar = 10 µm). Colocalization was quantified on 3D image stacks for transfected cells (n= 25 cells for SDHA and n= 23 cells for Calregulin) by intensity correlation analysis (ICA) using ImageJ software. The degree of colocalization is based on the intensity correlation quotient (ICQ) and Pearson's correlation coefficient (Rr). ICQ value ranges from -0,5 (segregation of the signal) and 0,5 (perfect overlap); an ICQ = 0 relates to a random distribution. A perfect linear correlation for Rr is shown at +1. The last image is pseudo-coloured image representing ICA with yellow representing high co-localization.

(B and D) Plots of the PDM values (Product of the Differences from the Mean), the axes on the plots are the PDM values on the x-axis and the red or green intensity on the y-axis (Li *et al., J Neuroscience* 2004) and a magnification of 10 µm of transfected cells.

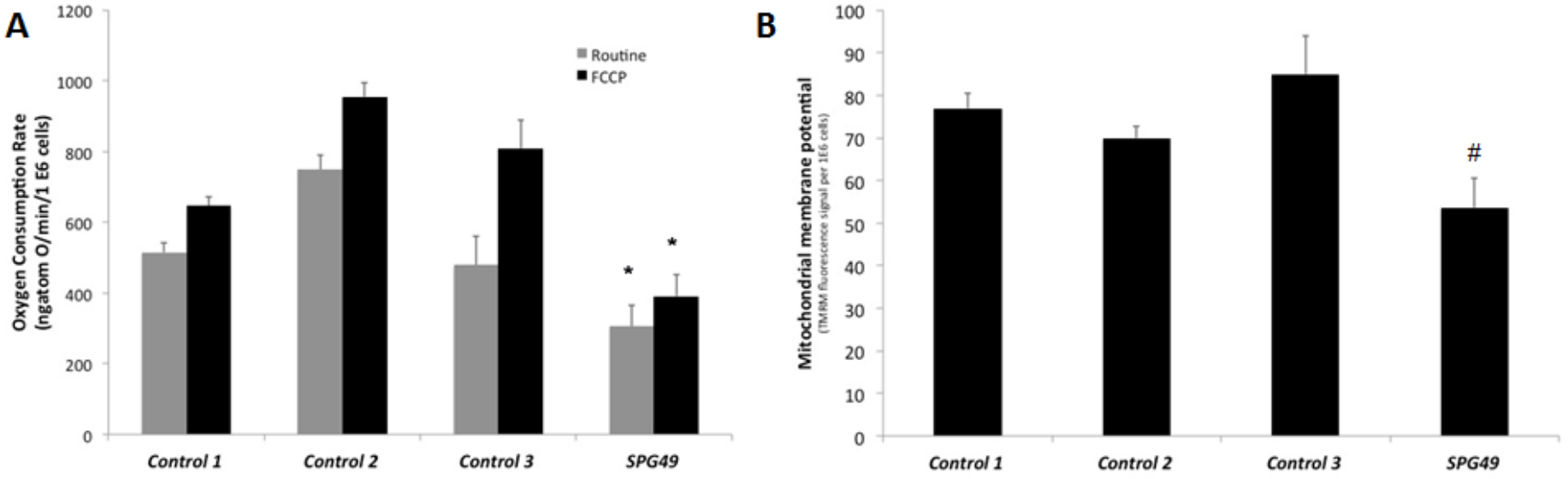

Figure S8. Investigation of Mitochondrial Bioenergetics in SPG49 Fibroblasts (Subject HSP1363-IV.1)

(A) Cell respiration was measured on intact cells under routine conditions (gray bar) or uncoupled state (black bar) in DMEM, and expressed as ngatom O / min / mg. SPG49 fibroblasts respiration was compared to that of three controls.

(B) Mitochondrial transmembrane electric potential (Δψ) was measured at steady-state in cells loaded with tetramethylrhodamine methyl esther (TMRM) and placed in DMEM at 37°C in a fluorometer. The fluorescence signal (arbitrary units normalized to $1^{E}6$ cells) of the TMRM steady-state is presented.

The * and # symbols indicate a p value < 0.05 between the mutated subjects and each of the controls (independent t-tests). Error bars represent the SD.

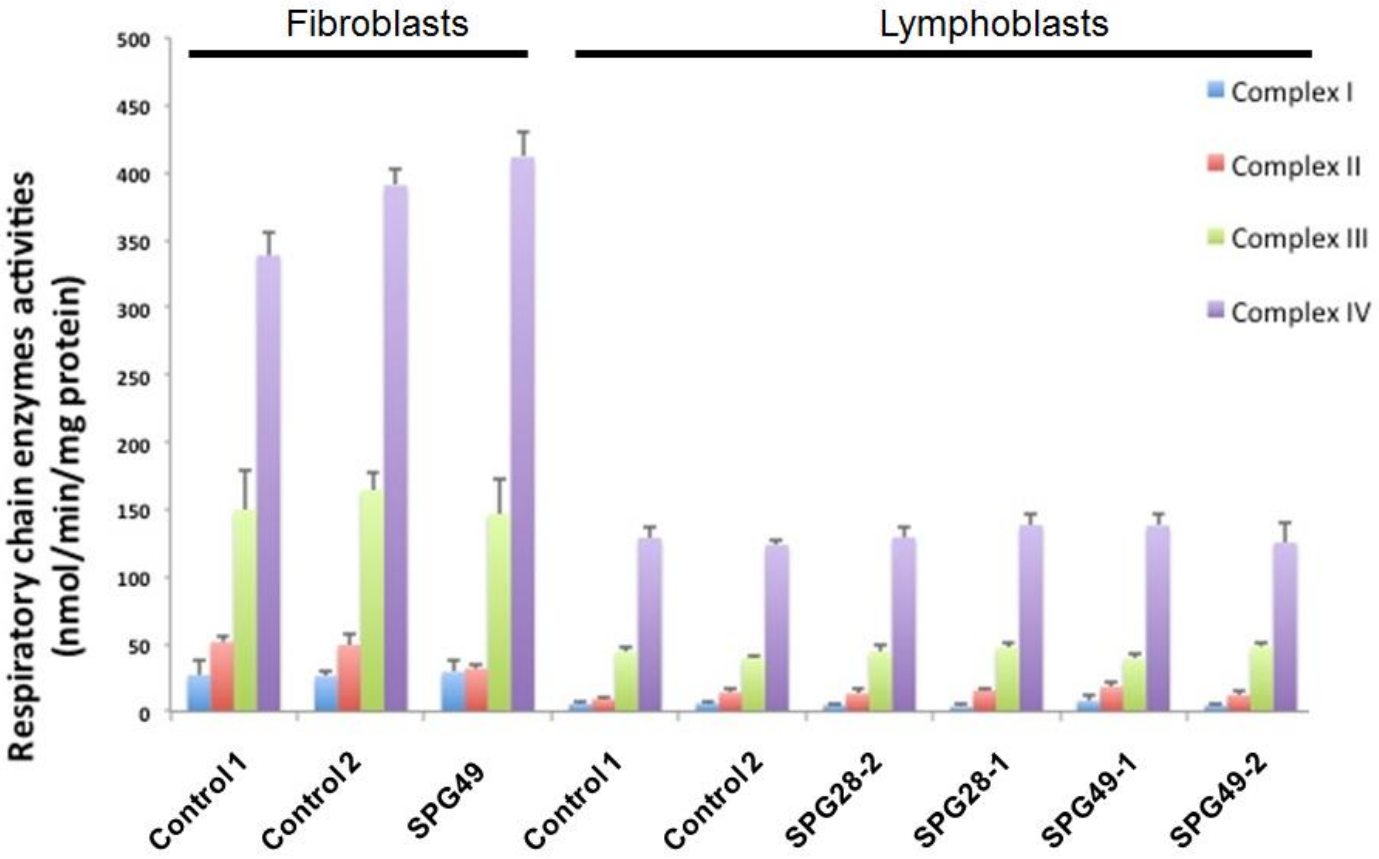

Figure S9. Investigation of the Enzymatic Activities of the Respiratory Chain in SPG28 and SPG49 Cells

Maximal catalytic activities (Vmax) of complex I, complex II, complex III and complex IV were measured by spectrophotometry on SPG28 or SPG49 fibroblasts and lymphoblasts compared to controls. The data are expressed as nmol/min/mg proteins. See Figure 3 legend for details on tested subjects. Error bars represent the SD.

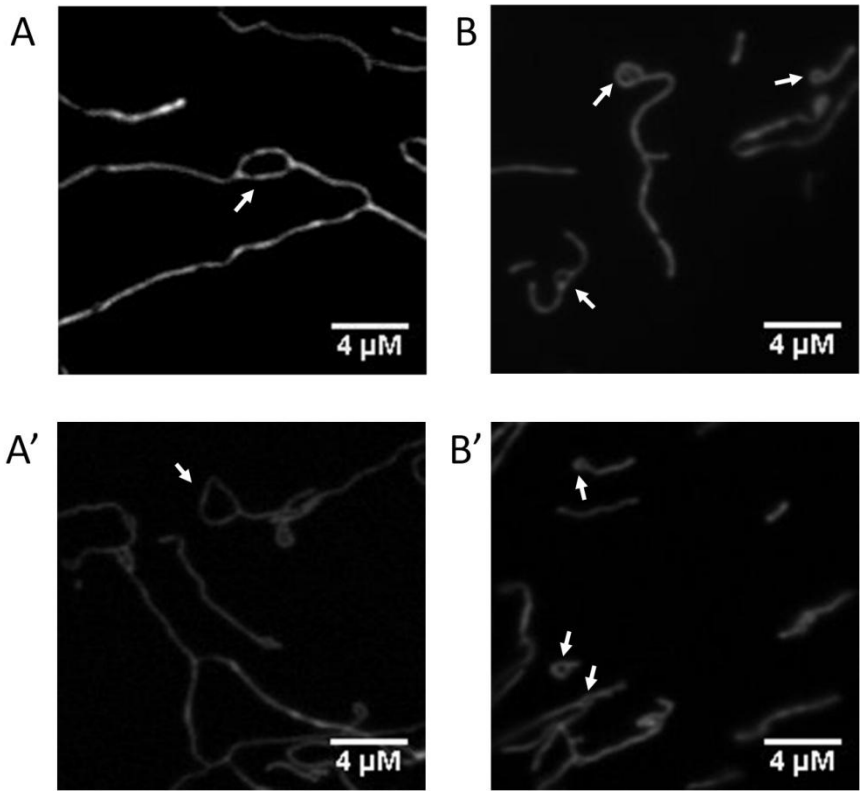

Figure S10. Mitochondrial Network Organization in SPG49 Fibroblasts

Human skin fibroblasts of an SPG49 individual (HSP1363-IV.1) were transfected with pCMV/mito/GFP vector (Invitrogen) in which the myc epitope was deleted (Darios et al*, J Neurochemistry* 2003), using the Neon system (Invitrogen) according to the manufacturer's instruction. Twenty four hours after transfection, live cells were observed on a Zeiss Axiovert 200 inverted video-microscope using 63X oil objective. Metamorph 7.7.7.0 software was used to acquire the image. Fibroblasts expressing a mitochondria-tagged GFP showed abnormal structures of the mitochondrial network. Both large circular subnetwork (A and A') and small donut-like vesicles (B and B') were observed as in another experiment in which the mitochondrial membrane was labeled with an anti-TOM20. This shows that donuts and subnetworks, highlighted by white arrows, are not corresponding to swallow mitochondria but real suborganization of the mitochondria network.

Table S1. List of *DDHD1* (NM_030637.2) and *CYP2U1* (NM_183075.2) Mutations

Gene	Mutation	Effect of the Mutation[#]	Absent in Control Chromosomes (n)	Absent in Exome Variant Server (Nb of Chromosomes)	Absent in GEM.app Exome Server (Nb of Chromosomes)*
DDHD1	**c.1249C>T**	**p.Gln417***	**180**	**13,006**	**-**
DDHD1	**c.1766G>A**	**p.Arg589Gln ; r.spl ?**	**894**	**13,006**	**-**
DDHD1	**c.1874del**	**p.Leu625***	**-**	**na**	**2,162**
DDHD1	**c.2438-1G>T**	**r.spl ?**	**180**	**13,006**	**-**
CYP2U1	**c.61_73del**	**p.Leu21Trpfs*19**	**636**	**na**	**2,170**
CYP2U1	**c.784T>C**	**p.Cys262Arg**	**1,222**	**13,006**	**-**
CYP2U1	**c.947A>T**	**p.Asp316Val**	**1,438**	**13,006**	**-**
CYP2U1	**c.1139A>G**	**p.Glu380Gly**	**572**	**13,006**	**-**
CYP2U1	**c.1462C>T**	**p.Arg488Trp**	**1,222**	**13,005 (one heterozygous subject, rs141431913)**	**-**

na : not applicable
* absent in exomes from 38 different phenotypes (https://genomics.med.miami.edu/gem-app/)
# checked at https://mutalyzer.nl/index